Origin and Suppression of Beam Damage-Induced Oxygen-K Edge Artifact from γ-Al_2O_3 using Cryo-EELS

Henry O. Ayoola[a], Cheng-Han Li[b], Stephen D. House[a,c], Cecile S. Bonifacio[a,1], Kim Kisslinger[d], Joerg Jinschek[b], Wissam A. Saidi[e] and Judith C. Yang[a,c,f,*]

[a]*Department of Chemical and Petroleum Engineering, University of Pittsburgh, Pittsburgh PA 15261, USA*
[b]*Department of Materials Science and Engineering, The Ohio State University, Columbus OH 43210, USA*
[c]*Environmental TEM Catalysis Consortium (ECC), University of Pittsburgh, Pittsburgh PA 15261, USA*
[d]*Center for Functional Nanomaterials, Brookhaven National Laboratory, Upton NY 11973, USA*
[e]*Department of Mechanical Engineering and Materials Science, University of Pittsburgh, Pittsburgh PA 15261, USA*
[f]*Department of Physics and Astronomy, University of Pittsburgh, Pittsburgh PA 15260, USA*
[1]*Present address: E.A. Fischione Instruments Inc., Export PA 15632, USA*

**Corresponding author. Tel.: +1 412 6248613.*

E-mail address: judyyang@pitt.edu (J. C. Yang).

Abstract

Gamma-alumina (γ-Al_2O_3), like other low-Z oxides, is readily damaged when exposed to an electron beam. This typically results in the formation of a characteristic pre-edge peak in the oxygen-K edge of electron energy-loss spectra (EELS) acquired during or after the damage process. This artifact can mask the presence of intrinsic O-K edge fine structure that would reveal chemical properties of the material; therefore, its suppression is key. In this work, we systematically investigate the conditions that give rise to the damage-induced O-K pre-edge peak and show that it can be effectively suppressed by performing EELS experiments at cryogenic (cryo) temperatures. Prolonged exposure of γ-Al_2O_3 to a focused electron beam results in a hole bored through the sample; this was used as a reproducible beam damage condition. O-K edge EELS spectra were collected from a single-crystal γ-Al_2O_3 sample both during and after focused

electron beam hole drilling, and at room and cryo temperatures, using a monochromated scanning transmission electron microscope (STEM). The characteristic 531 eV pre-edge peak visible in the room temperature EELS spectra was completely suppressed in the cryo-EELS spectra, even in the presence of a visible drilled hole. We then correlated these experimental observations with multiple-scattering EELS simulations to determine the likely atomistic origin of the damage-induced O-K pre-edge peak. The findings indicate that the pre-edge peak is caused primarily by the presence of surface O dimer (O-O) bonds formed during beam damage, and that operating at cryo temperature suppresses the formation of surface O-O bonds, thus preventing formation of the O-K pre-edge peak. Additionally, Al-$L_{2,3}$ edge EELS spectra revealed Al loss primarily from tetrahedral sites during hole drilling.

*Keyword*s: EELS; γ-Al_2O_3; beam damage; cryo-EELS; STEM

1. Introduction

Gamma-alumina (γ-Al_2O_3), one of several polymorphs of alumina, is an important industrial material that has been heavily studied due to its current and potential applications in catalysis [1, 2]. Among other tools, electron energy-loss spectroscopy (EELS) has been extensively used to study its chemical and electronic properties [3-5]. EELS uniquely provides chemical information at a spatial resolution beyond that of any other technique, rendering it ideal for studying features such as nanoscale surfaces and interfaces that are fundamentally important for catalysis. However γ-Al_2O_3, like many other Al-containing materials, is highly susceptible to beam damage by the electron probe [6]. Beam damage occurs in inorganic materials primarily by radiolysis, knock-on damage (sputtering), and electrostatic charging mechanisms [7-10]. These mechanisms can potentially alter the structure and chemistry of the material locally [9], which in turn can create artifacts in the EELS spectra that complicate or mislead data interpretation [11]. The presence of damage-induced artifacts has been noted to obscure other intrinsic EELS features of oxides, thus hindering analysis [5, 12]. For example, a beam damage-induced artifact was found to conceal the Ti-O bonding related pre-edge feature in Al_2TiO_5 [5].

It has so far been difficult to collect high-quality EELS data on such a beam-sensitive material as γ-Al_2O_3 without introducing artifacts. Previous EELS studies of Al_2O_3 [13] and K_2O-SiO_2 glass [14] encountered difficulty acquiring O-K edge spectra with high signal-to-noise (SNR) but minimal beam damage. Ordinarily, spectrum acquisition time or electron dose could be reduced to minimize the beam damage; however, this also has the unintended consequence of reducing the amount of signal collected and reducing spectrum quality, which limits accurate analysis of fine spectral features. Cryo-STEM—scanning transmission electron microscope (STEM)

experiments performed using specialized holders or microscopes that keep the sample at cryogenic temperature—is seeing growing use to suppress beam damage in sensitive materials such as biological samples [15-18] and, to a lesser degree, some inorganic samples [19-23]. For example, beam damage suppression has been demonstrated in some oxides using cryo-EELS [19, 24].

The oxygen-K edge EELS of beam-sensitive oxides including γ-Al_2O_3 is affected by electron beam damage in a well-recognized way, often through formation of a pre-edge peak. A pre-edge peak observed ~9 eV below the main O-K edge peak in magnesium aluminate ($MgAl_2O_4$) spinel was attributed to the formation of free O_2 by beam damage [14, 25]. Similarly, an O-K pre-edge peak at 531 eV was also seen in EELS spectra acquired from beam-damaged α-alumina [5] and attributed to O_2 gas bubbling under the focused electron beam. While the damage-induced pre-edge peak appears to occur at 531 eV, other pre-edge peaks closer to the edge onset of the O-K edge peak have differing sources. One such pre-edge peak has been associated with undercoordinated or dangling O atoms [26].

Although these previous studies point to the likely origin of the damage-induced pre-edge peak in beam-sensitive oxides, the exact source in γ-Al_2O_3 has not been explored. EELS simulations are useful to interpret spatially localized energy loss near-edge fine structure (ELNES) features [27], as is the case with the damage-induced O-K pre-edge peak. The use of *ab initio* ELNES calculations to interpret EELS spectra has been suggested as the next step in fully understanding the chemistry implicit in EELS [5]. One of the most well-used approaches to theoretical ELNES

simulation is the multiple scattering (MS) approach [28]. The MS approach is ideal for an aperiodic model such as would be expected in a disordered structure modified by beam damage. Accurate correlation of experiment and theory also requires that the material being examined and the simulation model are as identical as possible. The quality of commercially available γ-Al_2O_3, however, has made it difficult to directly correlate experimental results to simulations reproducibly. This is because commercial γ-Al_2O_3 is polycrystalline and often contains many different surface orientations and impurities (and potentially even amorphous material) [29-31], rendering it nonideal for direct comparison with simulations that have well-defined crystal structures and are free of impurities. The ideal sample for this study—a pure, well-defined, single-crystalline alumina with known surface orientations—is not normally produced commercially [32, 33].

In this work, the potential of cryo-EELS to suppress electron beam damage in γ-Al_2O_3 is investigated. Single-crystal γ-Al_2O_3 grown via thermal oxidation of single-crystal NiAl (110) [34] and both room-temperature and cryo-temperature monochromated STEM-EELS were used to systematically study the mitigation of beam damage-induced artifacts in the O-K edge ELNES of γ-Al_2O_3. Al-$L_{2,3}$ edge EELS was also acquired to more fully understand the beam damage process in γ-Al_2O_3. Subsequent correlative analysis of the experimental data with multiple scattering EELS simulations was employed to determine the likely atomistic source of the O-K pre-edge peak seen in beam damaged γ-Al_2O_3. This work builds upon the understanding of beam damage in beam-sensitive inorganic materials and proposes a method to suppress it, thereby enabling high resolution EELS studies to be performed.

2. Methods

2.1. Sample Preparation

Well-defined single-crystal (111) γ-Al_2O_3 was prepared by controlled thermal oxidation of NiAl (110) after the manner described by Zhang et al. [34] The surface of the NiAl was polished down to a grit of 0.05 μm and then cleaned with deionized water followed by gentle Ar plasma treatment. The NiAl was then oxidized at 850°C for 2 hours under 0.1 L/min of flowing dry air. Pt nanoparticles were deposited on the γ-Al_2O_3 surface and can be seen in some of the images but play no role in the reported work. Cross-sectional TEM samples were prepared using an FEI Scios dual-beam focused ion beam (FIB) operated at 30 kV, with final thinning at 5 kV and polishing at 2 kV.

2.2. Sample Characterization

Monochromated EELS data were acquired on an FEI Titan3^{TM} G2 60-300 S/TEM operated at 300 kV in parallel EELS mode, with collection and convergence angles of 18 and 10 mrad respectively. A Gatan Cryo-Holder cooled using liquid nitrogen to a working temperature of -186°C was used for the cryo experiments. EELS spectra were collected either as time series during the hole drilling, or as spectrum images after the hole drilling. EELS time series at cryo temperature were collected with an exposure time of 1s, while all other spectra were acquired with exposure times of 0.5 s. O-K edge EELS absolute edge onsets were calibrated using the position of the zero-loss peak (ZLP). Energy resolution calculated from the full-width half-maximum (FWHM) of the ZLP was about 0.3 eV in all acquired spectra.

2.3. Computational Details

EELS spectra simulations were carried out using FEFF9 [35, 36], an *ab initio* real-space multiple scattering (MS) code. Self-consistent field (SCF) potentials were calculated with a 6 Å cluster while full multiple scattering (FMS) was employed with an 8 Å cluster. The final state rule approximation was used to treat core-hole effects. Due to uncertainty in the calculated Fermi level caused by the muffin-tin potentials in FEFF, the absolute energy of simulated edges must be aligned to the experiment. Calculated O-K edge EELS spectra were aligned with the experimental EELS using "bulk" O atoms away from the surface of the model. The calculated spectrum for the bulk O atom was shifted to align the main O-K edge peak with the same peak in the experiment at ~541 eV. The FEFF calculated EELS spectra for the O-O dimer atoms were then shifted by the same value. The DFT calculations were carried out using the Vienna Ab Initio Simulation Package (VASP) [37, 38] in conjunction with Perdew-Burke-Ernzerhof (PBE) [39] exchange-correlation functional and Tkatchenko-Scheffler [40, 41] van der Waals corrections. Other computational parameters are described in the SI.

The γ-Al_2O_3 models containing surface O-O dimers were derived from the spinel-based models developed by Acikgoz et al [42]. Each model was the result of removing hydrogen from a different surface site before optimizing the structure. The bulk γ-Al_2O_3 model described by Digne et al. [43] was used to generate the drilled hole model.

3. Results

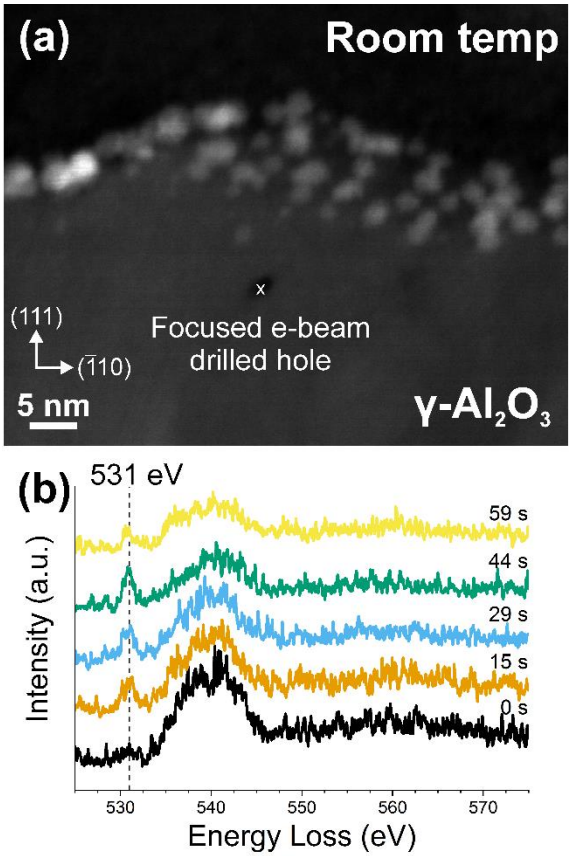

Figure 1. (a) Dark-field STEM image showing γ-Al_2O_3 sample. The position where the focused electron beam was used to drill a hole is marked with an x and labeled. (b) Time-resolved O-K edge EELS spectra acquired at room temperature during e-beam hole drilling. The characteristic e-beam damage-associated pre-edge peak at 531 eV as marked with the dotted line and labeled. The pre-edge peak intensity gradually increases and subsequently decreases with time.

A dark-field scanning transmission electron microscope (STEM) image of the cross-sectional sample is shown in Figure 1a. Pt nanoparticles can be seen on the surface, but these are not relevant for the present study. The TEM cross-section is covered by a carbon layer deposited during the FIB lift-out process. A hole has been drilled in the γ-Al_2O_3 at the position marked with an "x" using the focused electron beam at room temperature (RT). During the hole drilling,

an O-K edge EELS time series was acquired and is shown in Figure 1b. The characteristic O-K edge peak is seen, with a pre-edge peak also manifesting at the marked and labeled 531 eV position. The pre-edge peak intensity increases, reaches a maximum intensity, and then decreases with time during the hole drilling.

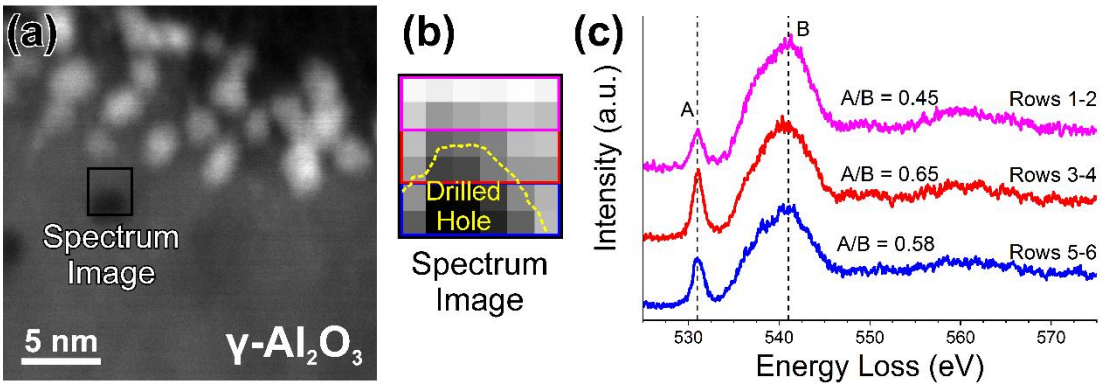

Figure 2. (a) Dark-field STEM image showing γ-Al_2O_3 sample after hole drilling at room temperature. An EELS spectrum image, marked by the box, was acquired around the hole edge. (b) Close-up of spectrum image showing individual pixels, each containing an EELS spectrum. The rough edge of the drilled hole is marked with the dotted line and labeled. The O-K edge EELS spectra in the pixels within each colored box were summed and displayed in (c). The O-K edge EELS spectra in (c) show the characteristic e-beam damage-associated pre-edge peak. The relative intensity of the pre-edge peak was calculated for each summed spectrum.

After the RT hole drilling, an EELS spectrum image was acquired also at RT from the region around the hole edge. A dark-field STEM image of the cross-sectional sample with a drilled hole in the γ-Al_2O_3 is shown in Figure 2a, with the area of spectrum image acquisition marked with the box and labeled. The close-up of the EELS spectrum image is shown in Figure 2b. Each pixel contains an EELS spectrum corresponding to that position. The edge of the hole is marked using the dotted line. The EELS spectra from the pixels in each box were summed and are plotted in Figure 2c. The pre-edge peak at the same 531 eV energy as seen in Figure 1 is also present. The

ratio of the intensity of the pre-edge peak in each summed spectrum relative to the main peak (A/B) is shown. The intensity of the pre-edge peak is higher in the summed spectrum from rows 3-4, which corresponds mostly to the edge of the hole, as shown by the calculated intensity ratio. The intensity of the summed spectrum from rows 5-6 is second highest; this area of the spectrum image encompasses a small section of the hole edge. The summed spectrum from rows 1-2 (that do not overlap with the hole) shows lowest intensity pre-edge peak.

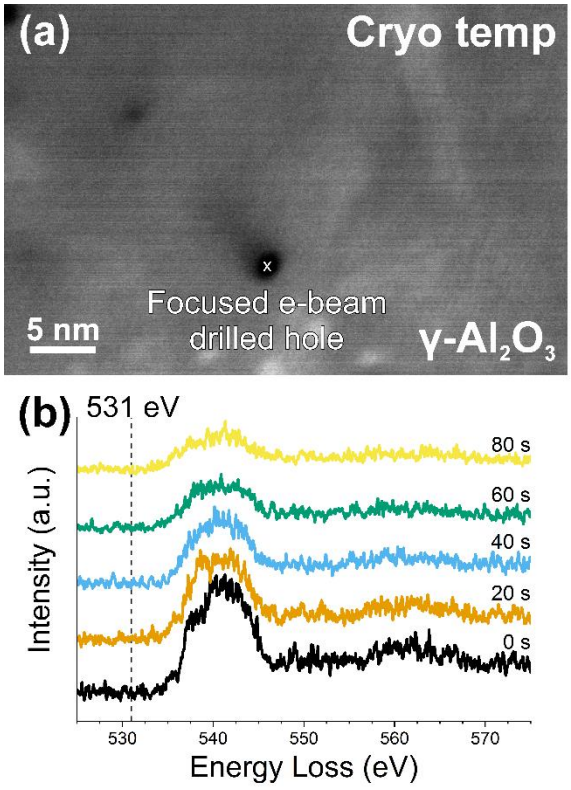

Figure 3. (a) Dark-field STEM image showing γ-Al_2O_3 sample. The position where the focused electron beam was used to drill a hole is marked with an x and labeled. (b) Time-resolved O-K edge EELS spectra acquired at liquid nitrogen temperature during e-beam hole drilling. The position of the characteristic e-beam damage-associated pre-edge peak at 531 eV is marked with the dotted line and labeled, but no pre-edge peak was seen at cryo temperature.

The hole drilling experiment was repeated in a new area of the cross-sectional sample, this time at cryo temperature (CT). The dark-field STEM image showing the drilled hole marked with an "x" in the γ-Al_2O_3 is shown in Figure 3a. An O-K edge EELS time series was also acquired during the hole drilling and is displayed in Figure 3b. No pre-edge peak was observed at any point during the CT hole drilling.

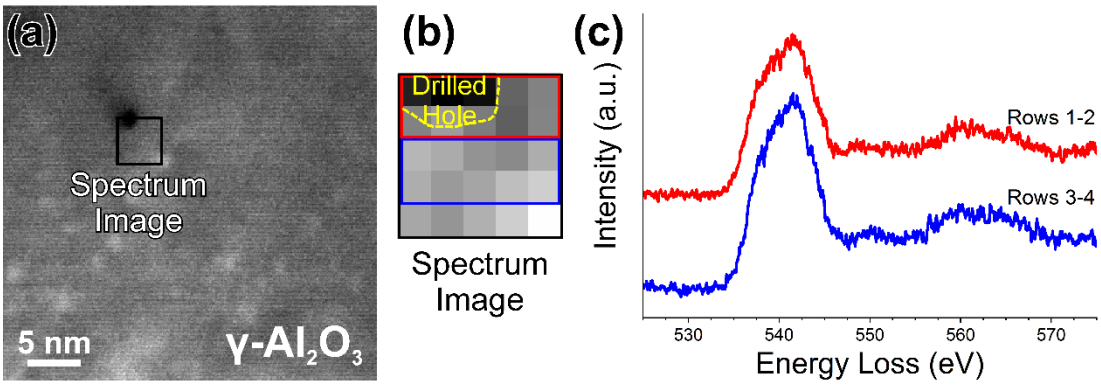

Figure 4. (a) Dark-field STEM image showing γ-Al_2O_3 sample after hole drilling at cryo temperature. An EELS spectrum image, marked by the box, was acquired around the hole edge. (b) Close-up of spectrum image showing individual pixels, each containing an EELS spectrum. The rough edge of the drilled hole is marked with the dotted line and labeled. The O-K edge EELS spectra in the pixels within each colored box were summed and displayed in (c). No pre-edge peak is seen in the O-K edge EELS spectra, confirming e-beam damage suppression during cryo temperature acquisition.

Mirroring the RT experiments, an EELS spectrum image was acquired after the CT hole drilling from the region around the hole edge. A dark-field STEM image of the drilled hole with the area of spectrum image acquisition marked with a box is shown in Figure 4a. The close-up of the spectrum image, with the edge of the hole marked, is shown in Figure 4b. The summed spectra from the enclosed pixels in the boxes in Figure 4b are shown in Figure 4c. No pre-edge peak was seen in the O-K edge EELS spectra around the edge of the CT drilled hole. The beam damage EELS experiments are summarized in Table 1.

Table 1. Summary of EELS experiments evaluating effects of beam damage on O-K edge EELS spectra at different temperatures.

Hole drilling O-K edge EELS observations	**200kV, RT**	**200kV, -186°C**
Hole formation with growing pre-edge peak	Yes	No
Hole formation with no pre-edge peak	No	Yes

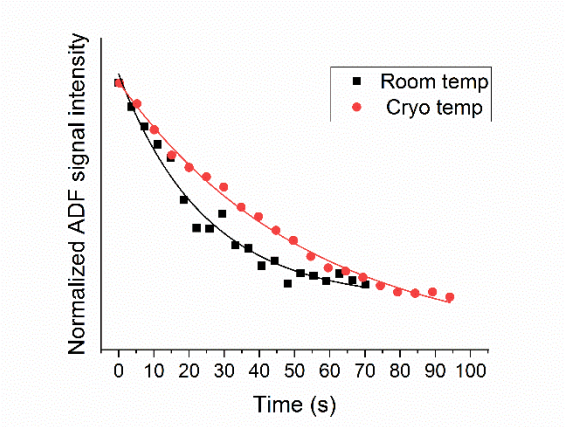

Figure 5. Hole drilling rates at room temperature and at cryo temperature determined by the normalized intensity of the annular dark field (ADF) detector signal during hole drilling. The exponential decay time constant at cryo temperature is longer than at room temperature, indicating a slower drilling rate at cryo temperature.

The rates of hole drilling during the beam damage experiments at RT and CT were estimated using the normalized intensity picked up by the annular dark field (ADF) detector during focused e-beam hole drilling and plotted in Figure 5. The hole drilling rates fit well to an exponential decay behavior (with R^2>0.97); faster at the start of the hole drilling and continuously decreasing with time. The exponential decay time constants are 53.9 s at CT and 24.7 s at RT.

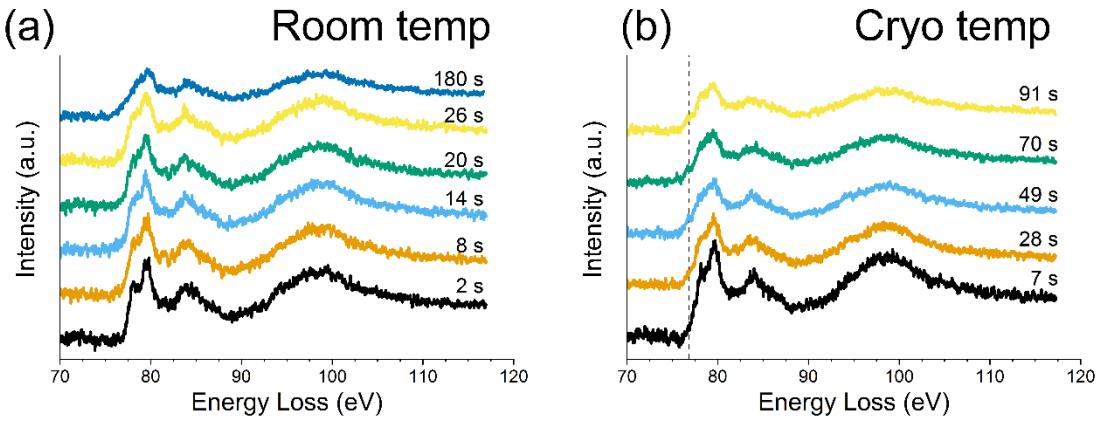

Figure 6. Time-resolved Al-$L_{2,3}$ edge EELS spectra acquired at (a) room temperature and at (b) liquid nitrogen temperature during e-beam hole drilling. The position of the increased pre-edge intensity at 77 eV is marked with the dotted line and labeled.

Additional hole drilling experiments were performed, with the Al-$L_{2,3}$ edge EELS acquired during the beam damage. The time-resolved Al-$L_{2,3}$ edge EELS acquired during hole drilling at RT and at CT are shown in Figure 6. The progression of the spectrum shapes is consistent between the RT and CT spectra, with the split peak at 79 eV transforming into a single asymmetrical peak during the course of hole drilling. At CT, a small pre-peak appears at about 77 eV during the beam damage experiment.

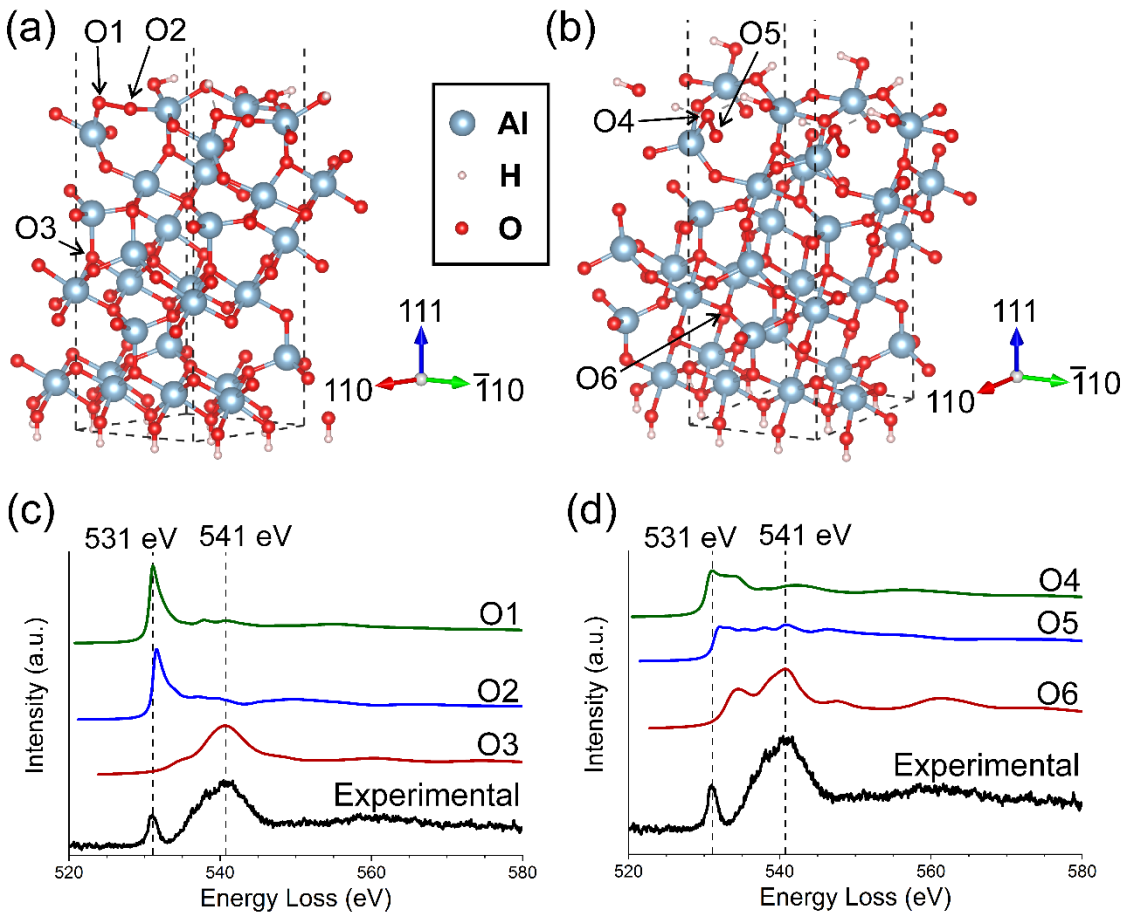

Figure 7. (a,b) Partially hydroxylated γ-Al_2O_3 (111) surface slab models with O atoms in the surface O dimers labeled O1 and O2 in (a) and O4 and O5 in (b). Bulk O atoms used for comparison are labeled O3 in (a) and O6 in (b). (c,d) Simulated O-K edge EELS spectra from the labeled O atoms in the models compared to the experimental O-K edge with beam damage-induced pre-edge peak. Simulated O-K EELS from O1-O2 (c) show the match of the peak positions with the beam damage-induced pre-edge peak. Likewise, simulated O-K EELS spectra from O4-O5 also show the match of the peak positions with the pre-edge peak.

Partially hydroxylated γ-Al_2O_3 (111) surface slab models containing a surface O dimer were used to perform EELS simulations to explain the origin of the O-K edge EELS pre-edge peak. The first surface model is shown in Figure 7a, with the O atoms of the O dimer labeled O1 and O2. A bulk O atom labeled O3 was used for comparison. The simulated O-K edge ELNES from O1-O3 are plotted in Figure 7c and compared to the experimental O-K edge EELS acquired from

the edge of the RT drilled hole. The positions of the peaks from the simulated O-K edge ELNES of the dimer O atoms align with that of the pre-edge peak seen in the experiment, while the simulated EELS from O3 aligns with the normal EELS O-K edge spectrum. ELNES simulations were performed on a second γ-Al_2O_3 (111) surface model containing a surface O dimer to confirm the results from the first model. The model is shown in Figure 7b, with the O atoms of the O-O dimer labeled O4 and O5, and a bulk O atom that was used for comparison labeled O6. The simulated O-K edge ELNES from the O atoms labeled O4-O6 are plotted in Figure 7d compared to the experimental O-K edge EELS. The peak positions from the simulated O-K edge ELNES of the dimer O atoms again align with the experimentally observed pre-edge peak.

4. Discussion

All EELS data were collected within the γ-Al_2O_3 only, sufficiently far away that the Pt could have no effect on the data. The O-K edge EELS time series data displayed in Figure 1b shows that the intensity of the O-K pre-edge peak associated with beam damage changes during the hole drilling. At the beginning of the focused beam experiment, the pre-edge peak is barely visible, since the damage has only just begun and is still minimal. 15 seconds later, the pre-edge peak intensity has increased to almost its maximum, highlighting the rapid damage that occurs in such a beam-sensitive material at RT. By 44 seconds, the pre-edge peak appears to be at its maximum intensity, almost at the level of the main O-K edge peak, which has itself begun to decrease in intensity due to loss of material at the point of the focused e-beam consistent with hole drilling. By 59 seconds, the intensity of the pre-edge peak has begun to diminish. The transient nature of the beam damage associated pre-edge peak has been observed in previous EELS experiments in other oxides [14, 26] and is consistent with the formation of O-related

phenomena that then escape the sample environment such as O_2 gas or bubbles, as has been proposed for complex oxides [5, 14].

The summed spectra from regions around the edge of the drilled hole shown in Figure 2c all show the pre-edge peak caused by beam damage. However, the spectrum from rows 3-4, which contains mostly the area around the hole perimeter, shows the highest pre-edge peak intensity as confirmed by the intensity ratio. It is important to note that the spectra in each pixel in Figure 2b were collected with a 0.5 s acquisition time, during which the liberation of O_2 gas would not be expected to generate as intense a pre-peak—particularly considering the pre-peak has a similar intensity to that in Figure 1b after 15 s of continuous exposure. This suggests that a significant contribution to the O-K pre-edge peak is an O-related structure that is more abundant on the perimeter of the surfaces formed by the beam damage, in addition to the liberation of free O_2 gas.

Additional support for the presence of damage-induced surface O species can be found in existing literature. EFTEM was used to show that the damage-induced pre-edge peak signal around a hole drilled in amorphous alumina was localized to the hole edge [44]. Prior study of ionization damage by Cazaux has suggested that radiolysis damage occurs on the sample surface first and progresses toward the bulk since electrons associated with surface atoms are less strongly bound [45]. These previous studies support the explanation that O species causing the pre-edge peak are found primarily on the beam-damaged surfaces. The transient nature of the pre-edge peak in Figure 1b can therefore be explained thusly; with the pre-peak intensity correlated to the perimeter of the drilled hole, the pre-peak intensity increases as the size of the

hole increases, eventually reaching a maximum and diminishing thereafter as the O_2 species on the surface are removed by the electron beam, perhaps as O_2 gas or bubbles.

It is important to consider the potential effect of scattering delocalization on the spatial resolution of the EELS spectrum images. Under the single scattering assumption, the delocalization due to inelastic scattering which is relevant for core-loss EELS was calculated using the formula provided by Egerton [46]:

$$(d_{50})^2 \approx \left(0.44\lambda/\theta_E^{3/4}\right)^2 + (0.52\lambda/\beta)^2$$

where d_{50} is the diameter containing 50% of the inelastically scattered electrons, $\theta_E \approx E/2E_0$ with E being the core-loss energy and E_0 the primary beam energy, and β is the EELS collection angle. The calculation gives an inelastic scattering delocalization diameter of 0.18 nm for the O-K edge, which is significantly smaller than the pixel size, and 0.77 nm for the Al-$L_{2,3}$ edge, which is approximately equal to the pixel size. Based on these calculations, it is safe to conclude that delocalization does not significantly affect our EELS analyses.

The spectrum image in Figure 2b also shows that the damage is not only in the area directly impinged upon by the beam, but also radiates outward from the point of the focused beam. The STEM image shows reduced intensity just outside the hole perimeter relative to the pristine γ-Al_2O_3, indicating material loss. Summed spectra from rows 1-2 which do not include the drilled hole still show the pre-edge peak caused by beam damage, albeit at a lower intensity. This indicates that significant radiation damage that modifies the structure of the material can occur in the vicinity of the electron beam just outside the volume of material being directly probed by the beam. While all the main damage mechanisms can have long-range effects, radiolysis is

expected to be the primary long-range mechanism since secondary electrons released by the initial beam interaction carry much of the transferred energy to then interact with further atoms in the sample [7, 47].

Figure 3 depicts a similar hole drilling experiment as the previously discussed, but at CT. The CT experiment proceeded in the same way as the RT experiment; after about 60 seconds of focusing the electron beam at a point, a hole was drilled in the γ-Al_2O_3. In this case however, there was no pre-edge peak seen in the O-K edge EELS time series acquired during the hole formation. The spectrum image acquired around the hole edge in Figure 4 also confirms the lack of an O-K pre-edge peak. This finding confirms that CT suppressed the formation of the surface feature that produces the pre-edge peak.

Since no pre-edge peak is seen at CT despite visible hole drilling, it is proposed that the source of the pre-edge peak is primarily a consequence of radiolytic processes, as has been previously suggested [6, 48]. Interestingly, the beam damage induced O-K pre-edge peak in a similar oxide was shown to have a dose-rate dependent threshold [26]. Here however, the dose rate is the same for both the RT experiment where the pre-edge peak is seen and the cryo experiment where no pre-edge peak is seen, suggesting an independent temperature effect in addition to the dose-rate effect. Operating at CT appears to suppress radiolytic beam damage as expected [7], while both knock-on damage and electrostatic charging which would be dose-dependent [8, 44] still occurs. This would explain why a hole is still drilled by the beam at CT, confirming the observations of Humphreys et al [44, 49].

A comparison of the first and last spectra of the O-K edge time series from both the RT (Figure 1) and CT (Figure 3) experiments (shown plotted together in Figure S1) shows no significant difference, suggesting no major difference in O coordination once pre-peak inducing O species have been formed and removed in the RT experiments. This also suggests Al must be simultaneously removed at a similar rate during beam damage, otherwise changes in O coordination would be expected. A slight increase in the intensity of the main peak at the edge onset in the CT spectra can be observed. This could be due to the increased presence of 3-coordinated O, as seen in EELS simulations reported by Ching et al [4]. However, it is difficult to compare the fine structure due to the decreased signal-to-noise in the later time series spectra.

The comparison of the early O-K edge spectra from the hole drilling time series between the RT experiment and CT experiments (shown plotted together in Figure S2) shows a slight difference of the fine structure in the main peak at 541 eV. The shape of the O-K edge acquired at CT (as shown with best signal-to-noise in Figure 4) closely resembles previously reported O-K edge EELS from γ-Al_2O_3 [50], suggesting the change is in the RT O-K edge. Small variations in fine structure can be seen at different timepoints in the RT O-K EELS time series, but the CT O-K edge EELS shape remains fairly consistent during the time series acquisition. Similar damage-induced fine structure fluctuations have been observed in damaged α-Al_2O_3 [5], suggesting small continuous changes in O coordination during hole drilling. That this damage is apparent in the first collected EELS spectrum highlights the difficulty of acquiring damage-free EELS spectra at RT from γ-Al_2O_3.

The hole drilling rates calculated from Figure 5 show exponential decay behavior; highest at the start of hole drilling and continuously decreasing with time. Hole drilling occurs more rapidly during pre-edge peak formation in the RT experiment as a result. Hole drilling also occurred faster at RT than at CT, as confirmed by the decay time constants. The entire exponential decay fit equations can be found in the Supporting Information. This is consistent with the reduction of beam damage by operating at CT that was observed in the EELS time series. Since radiolysis appears to be associated with the pre-edge peak formation, the suppression of radiolysis by operating at CT may correlate with the reduction of the hole drilling rate in the early stages of the CT hole drilling experiment. Interestingly, radiolysis is expected to be a more significant damage mechanism than knock-on for insulating materials [7, 51]. Since the damage rate is still significant even at CT, electrostatic charging may be a principal damage mechanism in γ-Al_2O_3, as has been proposed for some other oxides [10].

To gain deeper insight into the beam damage mechanisms occurring in γ-Al_2O_3, additional hole drilling experiments were conducted at both RT and CT, with Al-$L_{2,3}$ edge EELS time series acquired during the experiments and shown in Figure 6. At RT, the main observation is a gradual decay of the shoulder on the main peak at 79 eV with time. This peak has been assigned to the tetrahedral Al sites [4, 5] in γ-Al_2O_3, suggesting Al atoms on tetrahedral sites are preferentially removed, similarly to the beam damage observations in $MgAl_2O_4$ [52]. However, complete decay of the tetrahedral Al peak only occurs after long-time exposure to the beam (>3 minutes). At CT, the Al-$L_{2,3}$ edge changes in a consistent manner to the RT experiment, however there is an increase in pre-edge intensity seen more prominently in the CT experiment. The spectra containing the increased pre-edge intensity are strikingly similar to the Al-$L_{2,3}$ EELS of

amorphous Al_2O_3 and of $Al_2Ge_2O_7$ [5], which contains 5-coordinated Al atoms only. This suggests the presence of 5-coordinated Al and possibly other Al coordination types besides 4 and 6 in the beam damaged area. An explanation for this is that with knock-on and electrostatic charging being the main damage mechanisms, undercoordinated Al atoms that have lost O neighbors due to these damage mechanisms do not form new bonds before being sputtered away, and the increased number of 5-coordinated Al atoms can be detected. The increased pre-edge intensity is not observed at RT, where the undercoordinated Al atoms are able to form new bonds and the structure is able to rearrange during damage.

Multiple scattering EELS simulations were used to investigate the O-related surface feature formed during beam damage that produces the O-K pre-edge peak seen in the RT EELS experiments. Previous reports on other oxide materials suggested that the source of the pre-edge peak is the presence of O-O bonds [6, 14, 26]. A prior theoretical study of the (111) surface of γ-Al_2O_3 indicated some possible scenarios resulting in surface O-O bond formation, one such model finding that surface O-O dimers were formed after partial dehydration of a hydroxylated (111) γ-Al_2O_3 surface and subsequent relaxation [42]. Additionally, the cubic spinel-based model, the cubic model with Al atoms in spinel sites only, has been demonstrated to be the most accurate bulk model for γ-Al_2O_3 [53]. Thus, we use the partially hydroxylated spinel-based (111) surface model from the work by Acikgoz et al [42] for the subsequent EELS simulations. It is important to note that while the surface of the model is (111), the electron beam direction in the EELS simulations is the [110] direction of the model, to match the experimental setup.

The (110) and (111) surfaces of γ-Al_2O_3 are expected to be at least partially hydroxylated at RT [54]. Surface hydrogen removal or dehydration could potentially occur during electron beam irradiation and damage, through a form of electron-stimulated desorption [55]. Additionally, Al has a 4 times lower displacement energy (E_d) than O in the alumina framework [56], and it can be expected that Al atoms will be more rapidly displaced by knock-on during electron beam damage than O atoms. Electrostatic charging could also induce the migration of O anions into the irradiated area and the simultaneous migration of cations away [57]. These phenomena would have the effect of accumulating excess O atoms in the beam damaged area that would then potentially form peroxy O-O bonds more readily. Beam damage has also been observed to cause atomic restructuring in the probed material [58, 59] that could potentially in this case result in O-O bond formation. Further work however is required to determine the exact mechanism of O-O formation due to beam damage and is not further explored here. Instead, we focus on whether the presence of surface O-O dimers does in fact reproduce the O-K pre-edge peak.

The multiple scattering approach to simulating EELS spectra calculates the ELNES from a single absorbing atom at a time. Hence, the O-K ELNES from the O atoms in the O dimer (O1 and O2) in Figure 7a were simulated individually. The simulated ELNES shown in Figure 7c from both O dimer atoms consist of a sharp peak at the same position as the pre-edge peak from experiment. The simulated ELNES from a bulk O is plotted to check that the bulk O atoms indeed match the experimental peak position, thus confirming the results of the surface O dimer atom simulated O-K ELNES. For comparison, a model of the beam damage was created by simply removing atoms to form a hole from a bulk alumina model, similar to a model of the damage at CT without radiolysis damage. The O-K edge EELS was then simulated from the surface O atoms after

relaxing the atomic positions to the equilibrium structure (Figure S3). These simulations did not produce the pre-edge peak seen in the RT experiments. Based on these results, the presence of strong O-O bonds formed on the surface of the beam damaged γ-Al_2O_3 is proposed to be the likely source of the O-K pre-edge peak.

The O-O bond origin of the pre-edge peak was further confirmed by ELNES simulations from a second O dimer-containing surface model (Figure 7b,d). The simulated ELNES from the O dimer atoms show the edge onset at ~531 eV matching the experimentally observed pre-edge peak. However, these simulated ELNES also show additional fine structure after the sharp edge onset whereas those from the first surface model only show a sharp peak at ~531 eV (Figure 7c). This difference is likely because the O dimer atoms in Figure 7b are slightly below the surface and the O2 atom is bonded to two other Al atoms in addition to the O1 atom. This was confirmed by a third set of ELNES simulations from an O dimer-containing surface model (Figure S4). Both O atoms of the dimer in that model are bonded to two other Al atoms. Consequently, the simulated ELNES from the O-O dimer atoms in Figure S4 consisted of the sharp edge onset at ~531 eV and additional fine structure. We found that for the sharp peak to be produced at 531 eV, the O-O dimer atom should be bonded to only one other Al atom and should not be partially surrounded by other atoms.

In this work, we have shown that the use of cryo temperatures suppresses the formation of O dimers during the beam damage process, thereby suppressing the O-K pre-edge peak. Operating at cryogenic temperature appears to slow down the structure modification processes associated with radiolysis [9], which appear to contribute to the formation of surface O-O bonds. Knock-on damage, sputtering, and electrostatic charging however appear largely unaffected by temperature

reduction. Despite showing that surface O-O species produce the pre-edge peak, the contribution of O_2 gas released by the electron beam on the formation of the pre-edge peak cannot be completely ruled out. This is because the simulated O-K edge ELNES of the O dimer atoms appears similar to the O-K edge EELS reported for O_2 gas [12].

5. Conclusions

Through systematic EELS experiments at room and cryo temperatures, cryo-EELS experiments on γ-Al_2O_3 have been shown to be effective in reducing electron beam damage and suppressing the formation of EELS artifacts in the O-K edge resulting from structural modification primarily by radiolysis damage. This approach may be effective for other beam-sensitive inorganic materials such as other alumina phases and aluminum-containing compounds. The source of the beam damage associated O-K pre-edge peak has been proposed to be due to surface O-O dimers on the altered surfaces in the beam damaged area. EELS simulations have provided support for this hypothesis. Additionally, Al-$L_{2,3}$ EELS experiments have shown that Al atoms are preferentially removed from tetrahedral Al sites during beam damage in γ-Al_2O_3.
This work shows that specific artifacts in EELS spectra can be suppressed in a straightforward and repeatable way using a cryo-EELS that may be applicable to other materials with similar beam sensitivity problems. As a result, high quality can be collected while retaining sufficient SNR.

Acknowledgements

This work was supported by the National Science Foundation [CHE-1300544, CHE-1534630, CMMI-1905647 and DMR-1508417]; by DOE Basic Energy Sciences (DE FG02-03ER15476);

by the ETEM Catalysis Consortium (ECC) [funded through the University of Pittsburgh and Hitachi High Technologies], and by a start-up fund from the Department of Mechanical Engineering and Materials Science at the University of Pittsburgh. STEM and monochromated EELS data were acquired at the Center for Electron Microscopy and Analysis (CEMAS) at the Ohio State University (FEI Titan^{3TM} G2 60-300). DB-FIB sample preparation of the γ-Al_2O_3 sample was performed at the Center for Functional Nanomaterials, a U.S. DOE Office of Science Facility, at Brookhaven National Laboratory (BNL) under Contract No. DE-SC0012704. We are thankful to Dong Su and Eric Stach, both formerly of BNL, for preliminary data that developed into this work. We are thankful to Klaus van Benthem at UC Davis for access to cryo electron microscopy during the initial stages of this work. We are also thankful to Drs. Acikgoz and Pavanello for providing the γ-Al_2O_3 surface models from their paper. We are also grateful for computing time provided by CRC resources at the University of Pittsburgh.

References

[1] K. Wefers, C. Misra, Oxides and hydroxides of aluminum, in: Alcoa Technical Paper No. 19, Alcoa Laboratories, Pittsburgh, PA, 1987.
[2] M. Trueba, S.P. Trasatti, γ-Alumina as a Support for Catalysts: A Review of Fundamental Aspects, European Journal of Inorganic Chemistry, 2005 (2005) 3393-3403.
[3] I. Levin, A. Berner, C. Scheu, H. Muellejans, D.G. Brandon, Electron energy-loss near-edge structure of alumina polymorphs, in: Modern Developments and Applications in Microbeam Analysis, Springer, 1998, pp. 93-96.
[4] W.Y. Ching, L. Ouyang, P. Rulis, H. Yao, Ab initiostudy of the physical properties ofγ-Al2O3: Lattice dynamics, bulk properties, electronic structure, bonding, optical properties, and ELNES/XANES spectra, Physical Review B, 78 (2008) 014106.
[5] D. Bouchet, C. Colliex, Experimental study of ELNES at grain boundaries in alumina: intergranular radiation damage effects on Al-L23 and O-K edges, Ultramicroscopy, 96 (2003) 139-152.
[6] N. Jiang, J.C.H. Spence, In situ EELS study of dehydration of Al(OH)3 by electron beam irradiation, Ultramicroscopy, 111 (2011) 860-864.
[7] R.F. Egerton, Mechanisms of radiation damage in beam-sensitive specimens, for TEM accelerating voltages between 10 and 300 kV, Microsc Res Tech, 75 (2012) 1550-1556.

[8] R.F. Egerton, P. Li, M. Malac, Radiation damage in the TEM and SEM, Micron, 35 (2004) 399-409.
[9] L.W. Hobbs, Electron-beam sensitivity in inorganic specimens, Ultramicroscopy, 23 (1987) 339-344.
[10] N. Jiang, Electron beam damage in oxides: a review, Rep. Prog. Phys., 79 (2015) 016501.
[11] M. Nord, P.E. Vullum, I. Hallsteinsen, T. Tybell, R. Holmestad, Assessing electron beam sensitivity for SrTiO3 and La0.7Sr0.3MnO3 using electron energy loss spectroscopy, Ultramicroscopy, 169 (2016) 98-106.
[12] M.W. Ruckman, J. Chen, S.L. Qiu, P. Kuiper, M. Strongin, B.I. Dunlap, Interpreting the near edges of O2 and O2- in alkali-metal superoxides, Phys Rev Lett, 67 (1991) 2533-2536.
[13] D. Bouchet, S. Lartigue-Korinek, R. Molins, J. Thibault, Yttrium segregation and intergranular defects in alumina, Philos Mag, 86 (2006) 1401-1413.
[14] N. Jiang, J.C. Spence, Interpretation of Oxygen K pre-edge peak in complex oxides, Ultramicroscopy, 106 (2006) 215-219.
[15] L.A. Baker, J.L. Rubinstein, Chapter Fifteen - Radiation Damage in Electron Cryomicroscopy, in: G.J. Jensen (Ed.) Methods Enzymol., Academic Press, 2010, pp. 371-388.
[16] Z.J.W.A. Leijten, A.D.A. Keizer, G. de With, H. Friedrich, Quantitative Analysis of Electron Beam Damage in Organic Thin Films, The Journal of Physical Chemistry C, 121 (2017) 10552-10561.
[17] J.R. Meyerson, P. Rao, J. Kumar, S. Chittori, S. Banerjee, J. Pierson, M.L. Mayer, S. Subramaniam, Self-assembled monolayers improve protein distribution on holey carbon cryo-EM supports, Scientific Reports, 4 (2014) 7084.
[18] L.F. Kourkoutis, J.M. Plitzko, W. Baumeister, Electron Microscopy of Biological Materials at the Nanometer Scale, Annual Review of Materials Research, 42 (2012) 33-58.
[19] P. Torruella, C. Coll, G. Martín, L. López-Conesa, M. Vila, C. Díaz-Guerra, M. Varela, M.L. Ruiz-González, J. Piqueras, F. Peiró, S. Estradé, Assessing Oxygen Vacancies in Bismuth Oxide through EELS Measurements and DFT Simulations, The Journal of Physical Chemistry C, 121 (2017) 24809-24815.
[20] M. Ilett, R. Brydson, A. Brown, N. Hondow, Cryo-analytical STEM of frozen, aqueous dispersions of nanoparticles, Micron, 120 (2019) 35-42.
[21] H.M. Freeman, J.P.H. Perez, N. Hondow, L.G. Benning, A.P. Brown, Beam-induced oxidation of mixed-valent Fe (oxyhydr)oxides (green rust) monitored by STEM-EELS, Micron, 122 (2019) 46-52.
[22] X. Wang, M. Zhang, J. Alvarado, S. Wang, M. Sina, B. Lu, J. Bouwer, W. Xu, J. Xiao, J.-G. Zhang, J. Liu, Y.S. Meng, New Insights on the Structure of Electrochemically Deposited Lithium Metal and Its Solid Electrolyte Interphases via Cryogenic TEM, Nano Letters, 17 (2017) 7606-7612.
[23] Y. Li, Y. Li, A. Pei, K. Yan, Y. Sun, C.-L. Wu, L.-M. Joubert, R. Chin, A.L. Koh, Y. Yu, J. Perrino, B. Butz, S. Chu, Y. Cui, Atomic structure of sensitive battery materials and interfaces revealed by cryo–electron microscopy, Science, 358 (2017) 506-510.
[24] Y. Otsuka, Y. Shimizu, I. Tanaka, Beam damage suppression of low-κ porous Si–O–C films by cryo-electron-energy loss spectroscopy (EELS), J. Electron Microsc., 58 (2009) 29-34.
[25] K. van Benthem, H. Kohl, Methods for ELNES-quantification: characterization of the degree of inversion of Mg–Al-spinels, Micron, 31 (2000) 347-354.
[26] N. Jiang, J.C.H. Spence, On the dose-rate threshold of beam damage in TEM, Ultramicroscopy, 113 (2012) 77-82.

[27] R. Brydson, Multiple scattering theory applied to ELNES of interfaces, J. Phys. D: Appl. Phys., 29 (1996) 1699-1708.
[28] R.F. Egerton, Electron energy-loss spectroscopy in the electron microscope, Springer Science & Business Media, 2011.
[29] S.-H. Cai, S.N. Rashkeev, S.T. Pantelides, K. Sohlberg, Phase transformation mechanism between γ- and θ-alumina, Physical Review B, 67 (2003).
[30] Y. Liu, B. Cheng, K.-K. Wang, G.-P. Ling, J. Cai, C.-L. Song, G.-R. Han, Study of Raman spectra for γ-Al2O3 models by using first-principles method, Solid State Communications, 178 (2014) 16-22.
[31] X. Krokidis, P. Raybaud, A.-E. Gobichon, B. Rebours, P. Euzen, H. Toulhoat, Theoretical Study of the Dehydration Process of Boehmite to γ-Alumina, The Journal of Physical Chemistry B, 105 (2001) 5121-5130.
[32] Y. Li, C.M. Lousada, P.A. Korzhavyi, The nature of hydrogen in γ-alumina, Journal of Applied Physics, 115 (2014) 203514.
[33] T.N. Jensen, K. Meinander, S. Helveg, A.S. Foster, S. Kulju, T. Musso, J.V. Lauritsen, Atomic structure of a spinel-like transition Al2O3(100) surface, Phys Rev Lett, 113 (2014) 106103.
[34] Z. Zhang, L. Li, J.C. Yang, γ-Al2O3 thin film formation via oxidation of β-NiAl(110), Acta Materialia, 59 (2011) 5905-5916.
[35] K. Jorissen, J.J. Rehr, J. Verbeeck, Multiple scattering calculations of relativistic electron energy loss spectra, Physical Review B, 81 (2010) 155108.
[36] M.S. Moreno, K. Jorissen, J.J. Rehr, Practical aspects of electron energy-loss spectroscopy (EELS) calculations using FEFF8, Micron, 38 (2007) 1-11.
[37] G. Kresse, J. Hafner, Ab initio molecular dynamics for liquid metals, Physical Review B, 47 (1993) 558-561.
[38] G. Kresse, J. Hafner, Ab-initio molecular-dynamics simulation of the liquid-metal amorphous-semiconductor transition in germanium Physical Review B, 49 (1994) 14251-14269.
[39] K.B. John P. Perdew, Matthias Ernzerhof, Generalized Gradient Approximation Made Simple, Physical review letters, 77 (1996) 4.
[40] A. Tkatchenko, M. Scheffler, Accurate Molecular Van Der Waals Interactions from Ground-State Electron Density and Free-Atom Reference Data, Physical review letters, 102 (2009) 073005.
[41] W. Al-Saidi, V.K. Voora, K.D. Jordan, An assessment of the vdW-TS method for extended systems, Journal of Chemical Theory and Computation, 8 (2012) 1503-1513.
[42] M. Acikgoz, J. Harrell, M. Pavanello, Seeking a Structure–Function Relationship for γ-Al2O3 Surfaces, The Journal of Physical Chemistry C, 122 (2018) 25314-25330.
[43] M. Digne, Use of DFT to achieve a rational understanding of acid?basic properties of ?-alumina surfaces, Journal of Catalysis, 226 (2004) 54-68.
[44] S.D. Berger, I.G. Salisbury, R.H. Milne, D. Imeson, C.J. Humphreys, Electron Energy-Loss Spectroscopy Studies of Nanometer-Scale Structures in Alumina Produced by Intense Electron-Beam Irradiation, Philosophical Magazine B-Physics of Condensed Matter Statistical Mechanics Electronic Optical and Magnetic Properties, 55 (1987) 341-358.
[45] J. Cazaux, Correlations between ionization radiation damage and charging effects in transmission electron microscopy, Ultramicroscopy, 60 (1995) 411-425.
[46] R.F. Egerton, Limits to the spatial, energy and momentum resolution of electron energy-loss spectroscopy, Ultramicroscopy, 107 (2007) 575-586.

[47] R.F. Egerton, Scattering delocalization and radiation damage in STEM-EELS, Ultramicroscopy, 180 (2017) 115-124.
[48] J. Taftø, J. Zhu, Electron energy loss near edge structure (ELNES), a potential technique in the studies of local atomic arrangements, Ultramicroscopy, 9 (1982) 349-354.
[49] I.G. Salisbury, R.S. Timsit, S.D. Berger, C.J. Humphreys, Nanometer scale electron beam lithography in inorganic materials, Applied Physics Letters, 45 (1984) 1289-1291.
[50] I. Levin, A. Berner, C. Scheu, H. Muellejans, D.G. Brandon, Electron Energy-Loss Near-Edge Structure of Alumina Polymorphs, Modern Developments and Applications in Microbeam Analysis, 15 (2012) 93-96.
[51] R.F. Egerton, Choice of operating voltage for a transmission electron microscope, Ultramicroscopy, 145 (2014) 85-93.
[52] N. Jiang, J.C.H. Spence, Electronic ionization induced atom migration in spinel MgAl2O4, J. Nucl. Mater., 403 (2010) 147-151.
[53] H.O. Ayoola, S.D. House, C.S. Bonifacio, K. Kisslinger, W.A. Saidi, J.C. Yang, Evaluating the accuracy of common γ-Al2O3 structure models by selected area electron diffraction from high-quality crystalline γ-Al2O3, Acta Materialia, 182 (2020) 257-266.
[54] M. Digne, P. Sautet, P. Raybaud, P. Euzen, H. Toulhoat, Hydroxyl Groups on γ-Alumina Surfaces: A DFT Study, Journal of Catalysis, 211 (2002) 1-5.
[55] R.D. Ramsier, J.T. Yates, Electron-stimulated desorption: Principles and applications, Surface Science Reports, 12 (1991) 246-378.
[56] G.P. Pells, A.Y. Stathopoulos, Radiation damage in the cation sublattice of alpha-Al2O3, Radiation Effects, 74 (1983) 181-191.
[57] N. Jiang, J. Qiu, A.L. Gaeta, J. Silcox, Nanoscale modification of optical properties in Ge-doped SiO2 glass by electron-beam irradiation, Applied Physics Letters, 80 (2002) 2005-2007.
[58] M.R. McCartney, P.A. Crozier, J.K. Weiss, D.J. Smith, Electron-beam-induced reactions at transition-metal oxide surfaces, Vacuum, 42 (1991) 301-308.
[59] H. Gu, G. Li, C. Liu, F. Yuan, F. Han, L. Zhang, S. Wu, Considerable knock-on displacement of metal atoms under a low energy electron beam, Scientific Reports, 7 (2017) 184.